3b2 v7 OLEN : 2487 -
pp.1–16 (col.fig.: NIL)
PROD.TYPE: COM
ED: BINNY
PAGN: GNS SCAN: SHOBHA

ELSEVIER

Optics and Lasers in Engineering 0 (2001) 1–16

OPTICS and LASERS in ENGINEERING

Field measurements of volcanic gases using tunable diode laser based mid-infrared and fourier transform infrared spectrometers

Dirk Richter[a,b], Miklos Erdelyi[a], Robert F. Curl[a], Frank K. Tittel[a,*], Clive Oppenheimer[c], Hayley J. Duffell[c], Mike Burton[d]

[a] *Rice Quantum Institute, Rice University, Houston, TX 77251-1892, USA*
[b] *National Center for Atmospheric Research, 1850 Table Mesa Dr., Boulder, CO, 80305, USA*
[c] *Department of Geography, University of Cambridge, Downing Place, Cambridge, CB2 3EN, UK*
[d] *Sistema Poseidon, 95030 Nicolosi, Catania, Italy*

Received 21 March 2001; accepted 31 May 2001

Abstract

The first field measurements of volcanic gases using mid-IR difference frequency laser spectroscopy are reported. The results were obtained at the summit crater of Masaya volcano, Nicaragua, with the gases being drawn into a multi pass cell and measured at reduced pressure. Automated sensitive and selective detection of CO_2, SO_2, $H^{35,37}Cl$, H_2O, and CH_4 was achieved. Simultaneous measurements obtained with open-path Fourier transform spectroscopy provide a useful comparison of the two optical techniques. We also consider the potential measurement of CO_2 isotopic ratios in volcanic gases using laser-based spectroscopy.

Keywords: Mid-infrared absorption spectroscopy; Optical frequency conversion; Volcanic gases

1. Background and motivation

Volcanic eruptions are amongst the deadliest of natural phenomena and can involve landslides, pyroclastic flows, lahars, tephra falls, tsunami, and lava flows [1].

*Corresponding author. Fax: +1-713-348-5686.
E-mail address: fkt@rice.edu (F.K. Tittel).

0143-8166/01/$ - see front matter © 2001 Published by Elsevier Science Ltd.
PII: S0143-8166(01)00094-X

However, volcanoes rarely erupt without warning, if sensitive instrumentation is available to monitor the progress of magma towards the surface. The power of advanced volcano surveillance technology was demonstrated during the build-up to the climactic 1991 eruption of Mt. Pinatubo in the Philippines, in which measurements from a network of seismic sensors placed around the volcano signaled an impending eruption and enabled a timely evacuation of approximately 56,000 residents [2]. Also important in forecasting that a major eruption was on the way were measurements of high sulfur dioxide flux from the volcano.

Measurements of the fluxes and ratios of different volcanic gas species (e.g., SO_2, HCl, CO_2, etc.) can be especially powerful for interpretation of magmatic processes at depth. Since magmatic gases (released from bodies of molten rock beneath a volcano) can react with rocks and other fluids on their paths to the surface, determinations of isotopic ratios in the emitted gases can further assist in detecting the progress towards eruption [3].

Observations of volcanic gas emissions are also important for atmospheric science. Explosive eruptions represent the principal perturbation to the stratospheric aerosol burden. Even non-eruptive *fumarolic* emissions contribute a significant fraction of the background tropospheric sulfate burden. When they are deposited at the Earth's surface, volcanic volatiles can result in significant impacts to terrestrial and other ecosystems through acidification and toxification [4].

Compact and robust sensor technology is a critical requirement for volcanic gas monitoring, as equipment is often exposed to hostile conditions such as high humidity, large temperature fluctuations, and fumigation by acid gases. Furthermore, it is desirable for a volcanic gas sensor to operate unattended, without maintenance over long time periods to establish baseline behavior and identify significant excursions in gas composition. An ideal system would operate autonomously and remotely using an internet protocol. The sensor technology must further provide high selectivity, in addition to sensitivity, in order to identify specific emitted volcanic gas species. For this purpose, a new gas sensing technology based on direct mid-infrared absorption spectroscopy was developed [5] and deployed in a field experiment at Masaya volcano, Nicaragua. This volcano was chosen for its strong gas emission and relatively easy and safe access to the summit region, permitting us to evaluate the potential of portable spectroscopic gas sensors based on difference frequency generation (DFG) applied to real-time, sensitive and selective monitoring of emitted volcanic gas species. Simultaneous measurements were performed by open-path Fourier-transform infrared (FTIR) spectroscopy, which can measure a number of gas species of volcanological interest [3].

1.1. Masaya volcano

The Masaya volcano, at 625 m above sea level, is enclosed by a Nicaraguan National Park, and located $\sim$40 km south of the capital, Managua. The volcano's summit crater is easily accessible by road vehicle. A road runs around half of the 500 m diameter crater rim, enabling extractive and open-path sampling of the

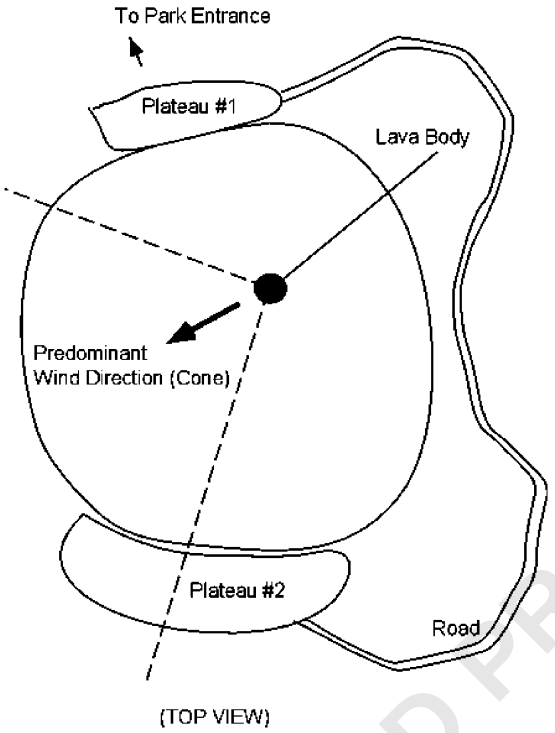

Fig. 1. The Santiago crater of Masaya volcano, Nicaragua. Indicated are the measurements locations and predominant wind direction during the field experiment in April, 2000.

volcanic plume, which is emitted from an incandescent vent on the floor of the crater (Fig. 1).

The last minor explosion at Masaya was reported in 1997 [6]. More significant is the persistent and strong degassing. Recent measurements indicate emission rates of $\sim 7.5\,\mathrm{kg\,s^{-1}}$ for HCl and $21\,\mathrm{kg\,s^{-1}}$ for SO_2 [6]. The latter figure compares to the anthropogenic release of SO_2 from whole of the United Kingdom of $55\,\mathrm{kg\,s^{-1}}$ [7].

Masaya's plume is heterogeneously distributed into the atmosphere as a result of local wind and weather conditions. While they can be useful for considering environmental and health impacts, measurements of the concentration of a single species are of no value in understanding volcanic activity. Much more informative are ratios of species such as HCl/SO_2 or CO_2/SO_2, as well as isotopic ratios such as $H^{35,37}Cl$. For example, a few weeks prior to a major eruption of Mt. Asama, Japan, a 30-fold increase in S : Cl ratios was measured [8]. Measurements of molar or isotopic ratios should be independent of the atmospheric gas distribution unless reactions occur in the plume. Open-path FTIR spectroscopic studies up to 15 km downwind from Masaya's crater have indicated negligible change in molar ratios of HCl and SO_2, despite the high atmospheric humidity. This suggests a comparable

dilution rate for SO_2 and HCl and gives confidence that summit measurements accurately reflect the volcanic source.

A precise measurement of the ratio of the two stable carbon isotopes of CO_2 ($^{13}CO_2$ and $^{12}CO_2$) can provide valuable information about CO_2 exchange processes in the volcanic plume. Changes in the isotopic ratio could be either explained by variations in the volcanic source, mixing with or anthropogenic sources (e.g., agricultural or industrial) as well as photosynthesis [9], or could manifest global and local changes. The natural abundance of ^{13}C is around 1%, but shows strong temporal and spatial variations.

Instead of the ratio, the abundance of ^{12}C and ^{13}C is usually given as a delta value and "per mil" unit defined by

$$\delta(‰) = \left(\frac{^{13}C_{sample}/^{12}C_{Sample}}{^{13}C_{std}/^{12}C_{std}} - 1 \right) \times 1000,$$

where the reference standard has been Belemnite of the Pee Dee Formation in South Carolina, US (PDB), with $^{13}C_{std}/^{12}C_{std} = 0.011237$ [10].

Mass spectroscopy is a standard method for measuring the isotopic ratio with high accuracy (0.1‰ or better), however it is not suitable for field measurements due to its large physical size [11] and tedious calibration routine. Direct absorption spectroscopy methods in the overtone regime (1.6 μm) [12,13], and using fundamental vibrational–rotational lines (4.3 μm) [14,15] by means of cryogenically cooled tunable narrowband diode lasers (TDL) were reported recently.

2. Optical instrumentation for volcanic gas concentration measurements

Two gas sensor technologies were applied to the detection of volcanic gas species at Masaya volcano, Nicaragua. Development and detailed performance characteristics of the DFG-based gas sensor have been reported by Richter et al. [5].

2.1. Automated DFG-based multi-component gas sensor

A widely tunable mid-infrared source is based on difference-frequency converted near-infrared diode lasers using quasi-phase matched periodically poled lithium niobate (PPLN). For spectroscopic applications, this new light source offers key advantages such as narrow-linewidth, coarse wavelength tunability, and reproducible fast linear mid-IR wavelength scanning. The use of passive and active optical fiber components allows a rugged design, efficient operation and compactness. Fig. 2 shows the optical architecture of the DFG-based gas sensor. Two near-IR diode laser sources are both pigtailed to a single mode fiber and the distributed Bragg reflection (DBR) diode laser operating at 1083 nm amplified to $\sim$500 mW using a Yb-doped fiber amplifier [16]. Wide tunablity is achieved with an external cavity diode laser (ECDL) (814–870 nm). Both fibered near-IR beams are imaged from a single-mode optical fiber into a 20 mm long PPLN crystal to generate mid-IR light

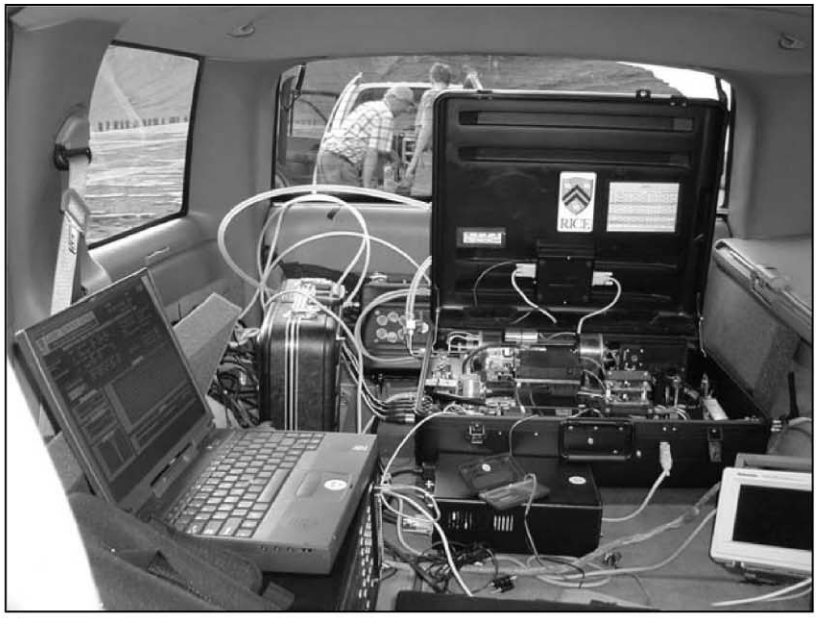

(a)

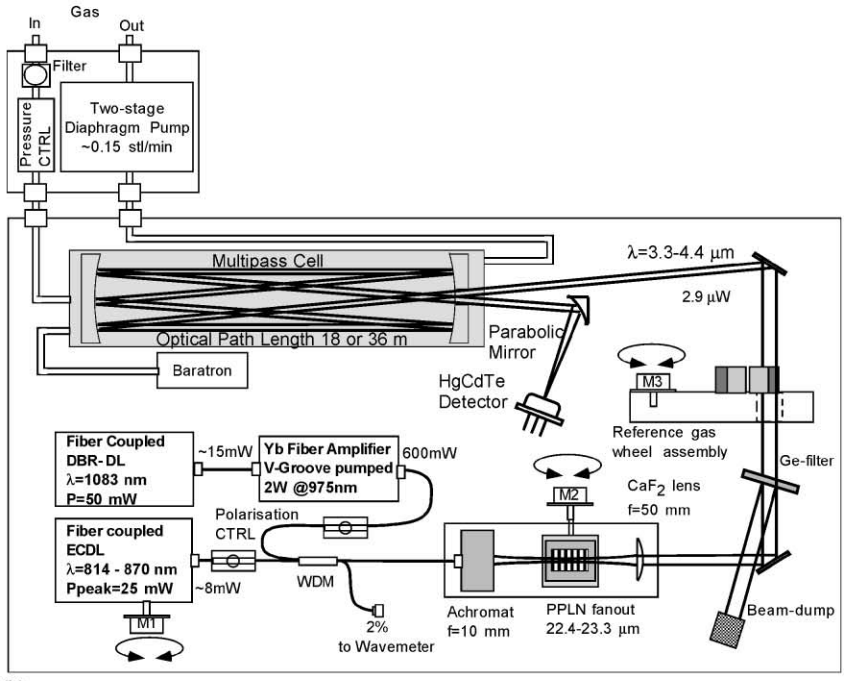

(b)

Fig. 2. (a) DFG-based gas sensor system in the rear compartment of a sport utility vehicle at Masaya's crater rim. (b) Configuration of the automated DFG-based multi-component gas sensor.

via a second-order parametric non-linear interaction. Phase-matching of the three optically dispersing interacting waves is achieved with an embedded phase-shift by periodic poling of the non-linear index. The PPLN crystal was designed with a fan-out poling period to offer continuous quasi-phase matching from 3.3 to 4.4 μm. Such a fiber based DFG source offers inherent optical alignment and beam pointing stability, spatial beam overlap and Gaussian pump beam quality leading to a high mid-IR conversion efficiency ($\sim 0.4\,\mathrm{mW\,W^{-2}\,cm^{-1}}$ at 3.3 μm [20]). Automatic and synchronous tuning of the ECDL and fan-out PPLN provide rapid mid-IR spectral tuning and can be used to account for instrumental wavelength drifts resulting from temperature fluctuations. Fig. 3 shows a flow chart diagram depicting the automatic acquisition sequence of the DFG-based gas sensor.

2.2. FTIR

We used a $0.5\,\mathrm{cm^{-1}}$ resolution spectrometer fitted with an indium antimonide (InSb) detector. Details of the instrument, field data collection and analytical methods are summarized in [3,4]. Retrievals were performed for spectral regions of approximately 100 wavenumbers around absorption features of interest by using a forward model [17] to simulate transmittance spectra for the atmospheric path, using the HITRAN96 database of spectral line positions and strengths. We then found the best fit to the field data using an optimal estimation, non-linear, least-squares algorithm [18].

An advantage of DFG-based gas sensing over FTIR spectrometers is its real-time quantitative response (2–10 s) and selectivity (40 MHz). The field portable FTIR instrument offers a resolution of 15 GHz and, at present, the acquired data require post-processing to determine measured gas concentration levels. On the other hand, the FTIR spectrometer covers a much wider wavelength range from 1.7 to 20 μm (requiring a change of detectors, MCT or InSb, and InAs) and can capture absorption signatures of many molecules in a short acquisition time (0.5 s for a single scan). Table 1 shows the performance characteristics of both sensor technologies.

3. Experimental details

The tunable DFG-based gas sensor shown in Fig. 2, together with support equipment, was shipped to Nicaragua and tested at a base camp located at the foot of the volcano. Mechanical sensors that were attached to the DFG sensor's shipping case indicated a shock exposure of at least 25 g. Operation of the DFG-based gas sensor was achieved in about 45 min (including test of individual photonic components). All fiber optic connections, DFG conversion optics and multi-pass cell [19] required no adjustment.

For measurements at the crater rim, the DFG-based gas sensor was placed in the rear compartment of an air-conditioned vehicle (Fig. 2). Electric power was provided by a portable petrol-engined generator ($P_{\max} = 1000\,\mathrm{W}$). The generator was placed approximately 30 m downwind to avoid or minimize the detection of its exhaust.

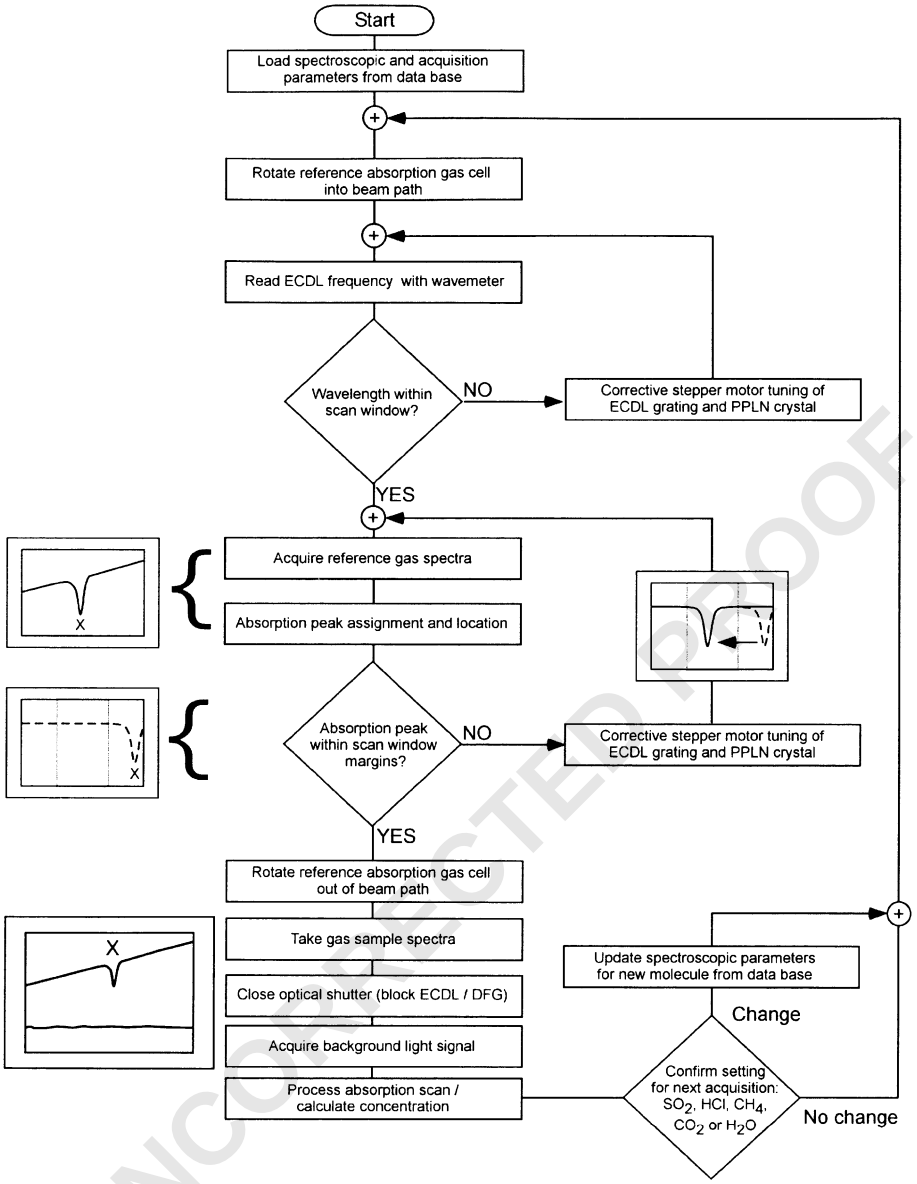

Fig. 3. Flow chart of a typical spectroscopic acquisition sequence with a DFG-based gas sensor.

Ambient air was sampled at a rate of $\sim 0.2\,\mathrm{l\,min^{-1}}$ through a 4 m long teflon tube (1.28 cm diameter) mounted to a pole outside the vehicle. Weather conditions during the April 2000 measurement campaign included maximum outside temperatures ranging from 32°C to 38°C and relative humidity levels from 60% to 90%. At all times, the vehicle engine was operating at idle speed to power the air conditioning.

Table 1
Performance characteristic of mid-IR sources applied to absorption spectroscopy

	Open path fourier transform infrared spectrometer (FTIR)	Extractive diode laser based DFG gas sensor
Sensitivity (absorption)	10^{-4}	10^{-4}
Selectivity (MHz)	15,000	40
Coarse tuning (cm^{-1})	625–6500	2270–3030
Fine tuning (cm^{-1})	N/A	>2
Response time (s)	0.5	2–60
Data processing	Post	Automatic, near real time (1–2 s)

However, the temperature was not actively regulated, and so varied as cloud cover and outside temperature changed. The vehicle was positioned such that its exhaust pipe faced downwind, away from the sampling inlet. Measurements were taken at both Plateaus 1 and 2 shown in Fig. 1, and volcanic gases were sampled according to the wind direction. Moving between the two locations required about 30 min to regain gas sensing operation. During our measurement campaign, the wind direction transported the plume predominantly towards the west, the one azimuth not well covered by the road around the crater, but we did sample concentrated volcanic plume on several occasions when the wind shifted favorably.

The sensors performed measurements over a 4-day period, ~8 h per day. During this period, the sensor operated mostly in automatic mode that included frequency locking of the absorption lines in the center of the absorption scans by means of stepper motor wavelength tuning. In the case of HCl and SO_2 monitoring, the detection sequence included the use of high concentration reference gas cells to determine the absorption peak location. Before taking a measurement, the reference gas cells were rotated into the beam path to enable the software to locate the position of the absorption line and distinguish from residual etalon peaks and baseline irregularities. The residual baseline noise of the sensor ranged from 0.1% to 0.2%. This is about a factor of two to five less sensitivity than typically achieved in laboratory measurements. The residual noise was dominated by an optical etalon and was later determined to be caused by the frequency modulated Yb-fiber amplifier pump channel.

During the 4-day measurement campaign, five gases including CO_2, SO_2, HCl, H_2O, and CH_4, were detected sequentially. Due to the wind conditions, the most useful measurements were performed on the last two days. SO_2 and HCl are considered to be solely volcanogenic, while CO_2, H_2O and are a mixture of volcanic plume and ambient air. CH_4 is a fairly common volcanic gas but FTIR spectroscopic measurements at Masaya have failed to detect it. Volcanic emissions are thought therefore to have contributed neglibly to the measured CH_4 concentrations.

Fig. 4 shows the measurement of CH_4 at Plateau #2 on April 14, 2000 during a 25 min time period. The standard deviation corresponds to 52 ppb, or an accuracy of 2.7%. The total accuracy is 7%, estimated from a comparison of the HITRAN96 spectroscopic database and our field spectra.

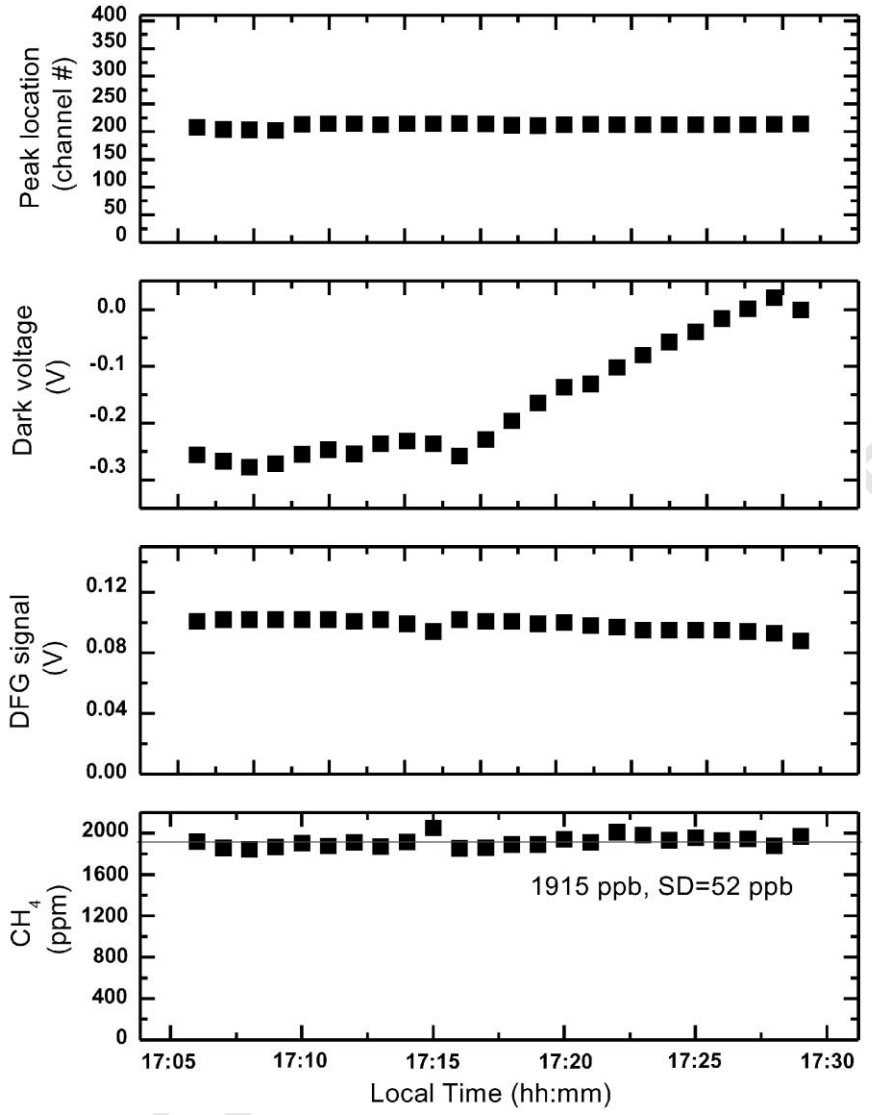

Fig. 4. Measurement of CH_4 at Masaya volcano, Plateau 2, April 14, 2000. Also shown are DFG signal, dark voltage and peak location, indicating a stable, nearly drift free time period. The estimated measurement accuracy is 7%.

On April 17, 2000, measurements of HCl and SO_2 were performed at Plateau #2. For the detection of HCl, the DFG-based gas sensor was tuned to 2843.6 cm^{-1}. Fig. 5 shows a rise in HCl concentration, reaching a maximum concentration of 175 ppb at 11:30 h. The concentration increased as the transport direction of the volcanic plume shifted towards the sampling location. Shortly before noon, the

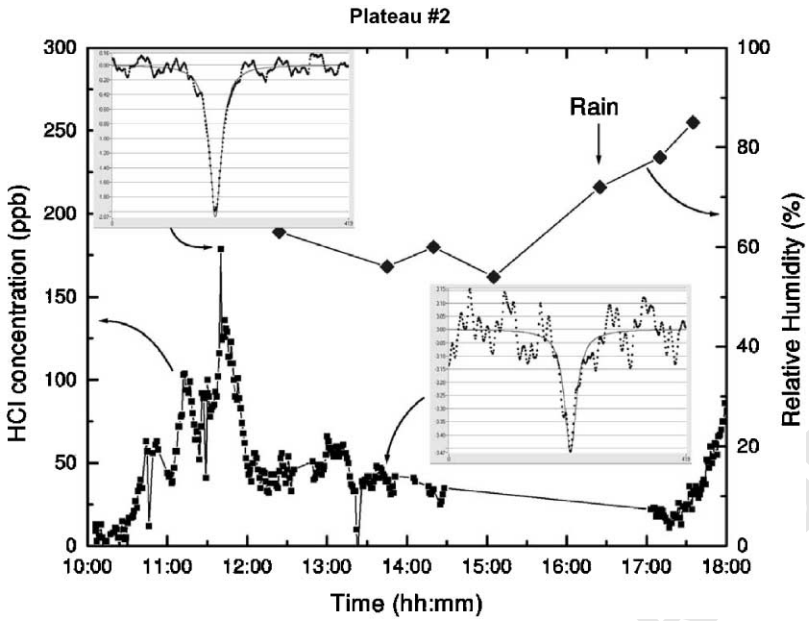

Fig. 5. Measurements of HCl emitted by Masaya volcano. Shown are sample spectra fitted to a Lorentzian lineshape function and humidity levels.

concentration sharply decreased to a level of ~ 50 ppb within 15 min. At 14:30 h, the DFG frequency was tuned to 2505.239 cm^{-1} to detect SO_2.

At 17:00 h, the sensor was tuned back for the detection of HCl at 2843.6 cm^{-1}. Also shown in Fig. 5 is the steady increase of humidity recorded with a digital hygrometer and indication of a short rain period at 16:30 h. Dense gas plumes continued to pass our sampling location and led to an increase of HCl, with a noticeable delay at 17:30 h. This delayed response can be attributed to chemisorption of the strongly polar HCl molecule to a water vapor film accumulated by rain and high humidity covering the inside of the teflon sampling tube.

The HCl spectra shown for two sample points indicate a residual baseline noise of $\sim 0.2\%$ corresponding to a sensitivity of ~ 15 ppb.

Between 14:30 and 17:00 h the DFG sensor was tuned to measure SO_2. For comparison, the FTIR instrument was set up for open-path measurements along the crater rim (Fig. 6). The FTIR spectrometer, optically joined to a 25.4 cm Newtonian telescope, was located by the vehicle and collected light from a Nernst glower placed 135 m downwind.

The results shown in Fig. 7 indicate close correspondence in the measured amount of SO_2 by the two techniques, within error margins given by the DFG-based gas sensor (3 ppm minimum detectable concentration for a signal-to-noise ratio of 1). Exact correspondence is not to be expected since the two instruments were sampling different regions of the plume.

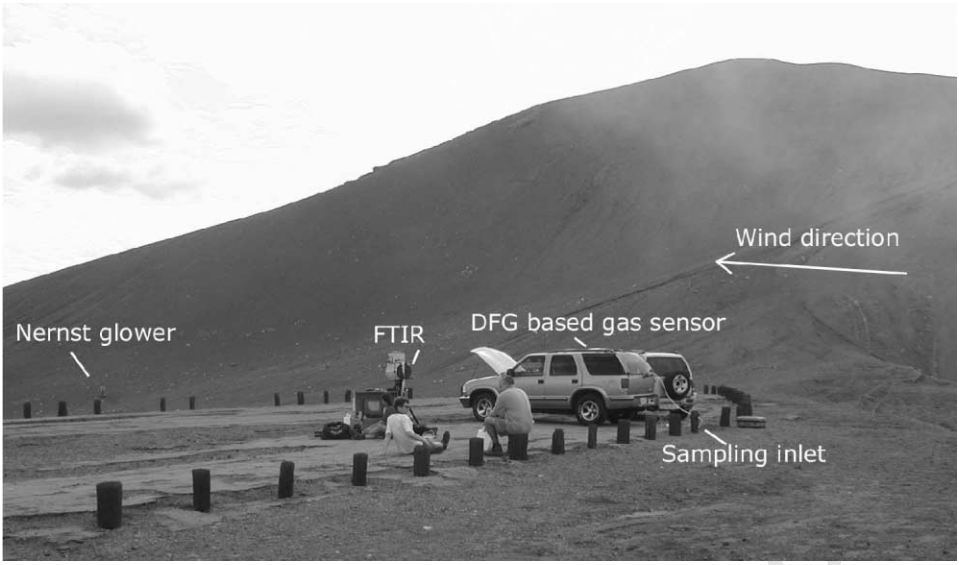

Fig. 6. Experimental arrangements of extractive DFG-based and open-path FTIR spectroscopy gas measurements at Plateau 2.

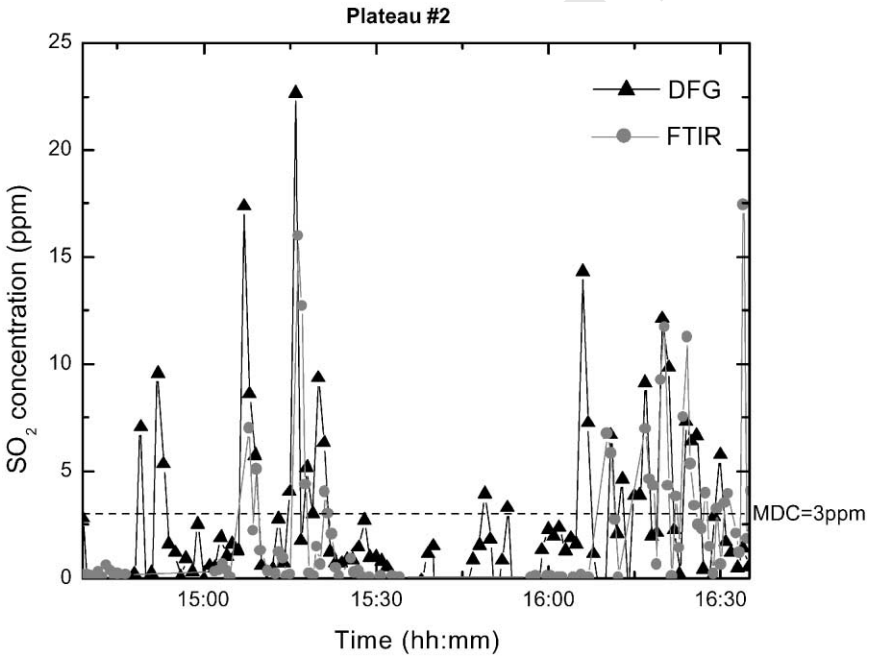

Fig. 7. Measurements of SO_2 emitted by Masaya volcano. Shown are the measured SO_2 concentrations of the extractive DFG-based gas sensor and open-path FTIR gas sensor.

Table 2
Summary of detected gas species, measured concentrations and field sensitivities of the multi-component DFG-based gas sensor

Gas species	DFG center frequency (cm^{-1})	DFG measured concentrations (Min–Max) ppm	Field sensitivity (MDC)	
			DFG	FTIR (mean)
CH_4	3028.751	1.85–2.05	32 ppb	419 ppb
CO_2	2388.640	374–567	3 ppm	30 ppm
H_2O	2649.348	18,000–21,200	670 ppm	710 ppm
HCl	2843.624	MDC–0.175	15 ppb	15 ppb
SO_2	2505.239	MDC–22.65	3 ppm	200 ppb

The overall performance of the DFG-based gas sensor indicates its suitability for field operation, even under unfavorable conditions such as high temperature and humidity. Table 2 summarizes the detected gas species and performance of DFG and FTIR gas sensors in a field application. Extractive gas detection of strongly polar molecules and associated chemisorptions and physisorption effects can have a substantial impact on the accuracy of the gas measurement, especially if humidity and a long sampling tubing act as a gas adsorber. The ratio of HCl and SO_2 as measured by the FTIR was ~ 1.5. This indicates that the DFG gas sensor measured two orders of magnitude lower HCl concentration levels than the FTIR. Although less selective, open-path gas measurement configurations perform, in this case, more accurately and permit accurate determination of the HCl/SO_2 ratio. Temperature-induced drifts in the detector and diode laser electronics introduce a limit on DFG instrument accuracy, and demand a high level of automatic control (i.e. wavelength drift compensation by stepper motor tuning). A better temperature management using a solid-state cooler could compensate for any ambient temperature cycling and would provide optimum continuous gas sensor performance.

Table 2 shows comparable detection sensitivities of the DFG and FTIR spectroscopic gas measurements. The field sensitivities for the DFG instrument were determined by the residual fit error to the baseline, while the FTIR spectroscopy sensitivities are expressed as mean values calculated from the errors of all measurements taken on April 17, 2000. The FTIR instrument accuracy for the absolute gas concentration was 10–20% and is determined by the measurement of the path length and by parameterization of the retrieval.

4. $^{13}CO_2/^{12}CO_2$ isotopic ratio measurements

This section reports on the development of a sensor for measurement of $^{13}CO_2/^{12}CO_2$ isotopic ratio in volcanic gases with a target accuracy of $\delta = 1‰$. The DFG-based light source described in Section 2.1 and depicted in Fig. 2 was used. However, the 36 m long multipass cell was replaced with a short, 20 cm long dual-beam cell (see Fig. 8) for the calibrated reference, and the sample gas, respectively.

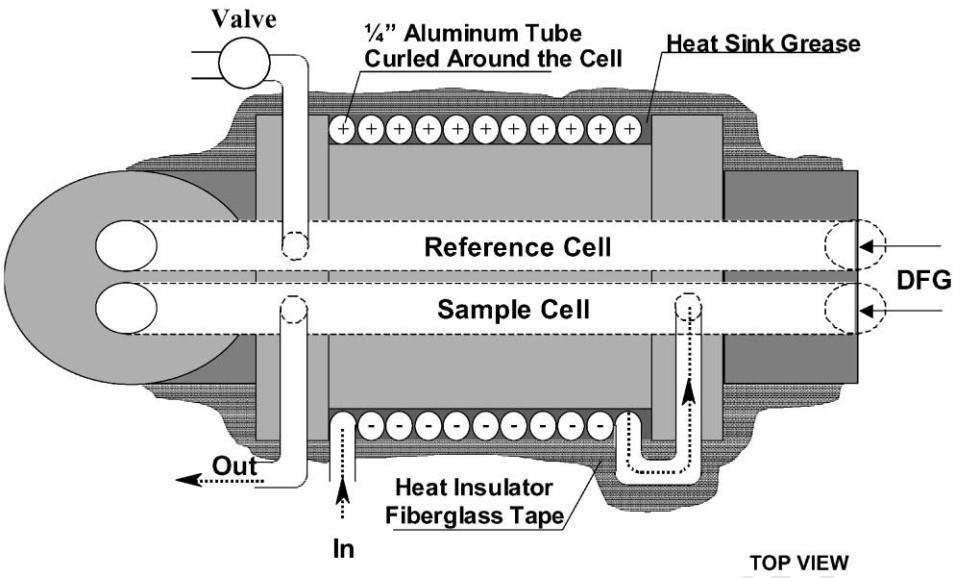

Fig. 8. Dual chamber gas sampling cell for precision isotopic ratio measurements of $^{13}CO_2/^{12}CO_2$. CaF_2 windows are at Brewster angle to minimize optical interference.

This section also details technical issues regarding line selection, temperature sensitivity and data analysis.

4.1. Line-pair selection

The strong vibrational–rotational absorption bands of $^{12}CO_2$ and $^{13}CO_2$ centered at 4.28 and 4.37 μm, respectively, provide several line pairs that are suitable for direct absorption spectroscopy. Our DFG-based light source described in the previous section can be tuned to these lines. However, due to the decreased power of the ECDL laser at this wavelength (867 nm), and the increased absorption of the PPLN crystal, the generated DFG power is 0.2 μW [20]. To select the most suitable line pair, the following conditions were taken into consideration:

(i) To minimize fitting errors, the intensity of the two $^{13}CO_2$ and $^{12}CO_2$ lines must be almost identical, and their spectral separation must be smaller than the scan range of the laser (typically 0.3 cm^{-1}) so that both lines should be in the scan-window.
(ii) The expected CO_2 concentration of fumarolic gases is around 10,000 ppm. To avoid saturation of the signal, the peak absorption should preferably be less than 50%.
(iii) Linear regression method (described in the next section) assumes that the $^{12}CO_2$ line(s) are spectrally separated from $^{13}CO_2$ line(s). Any interference between the two isotopic lines deteriorates the measurement.

The most suitable line pair that satisfies all the requirements listed above is centered at 2299.642 cm^{-1} ($^{12}CO_2$, P41) and 2299.795 cm^{-1} ($^{13}CO_2$, R22). The spectral separation of these lines is 0.153 cm^{-1} and their FWHMs at 100 Torr total pressure are 0.0177 cm^{-1} ($^{12}CO_2$) and 0.01859 cm^{-1} ($^{13}CO_2$). Owing to the very high CO_2 concentrations, (ii) can only be satisfied if the 36 m long multipass cell is replaced with a 20 cm long cell fitted with Brewster windows (see Fig. 8) to minimize optical fringing. The transmission of the lines is 61.2% ($^{12}CO_2$) and 50% ($^{13}CO_2$), respectively. Since these lines interfere with the same isotope only, the scan-window can be easily divided into two parts, one containing lines belonging to $^{13}CO_2$, and the other containing lines belonging to $^{12}CO_2$.

4.2. Temperature sensitivity

Since the natural abundance of ^{13}C is about 1%, the $^{12}CO_2$ line of the aforementioned line pair has to be a "weak line" (compared with other lines in the same branch), while the $^{13}CO_2$ line has to be a "strong line". In other words, to make the $^{12}CO_2$ line of comparable intensity, a low Boltzmann factor is required. It means that the lower energy level belonging to the $^{12}CO_2$ line is much higher (1340 cm^{-1}) than the lower energy level of the $^{13}CO_2$ line (197 cm^{-1}). Detailed calculations show that to measure the δ value with a precision of the order of, or better than 1‰, the temperature has to be stabilized with an accuracy of 50 mK. To achieve this small temperature difference between the reference and sample gases, the sample gas is directed through a 1 m long tube curled around the cell. The cell is thermally isolated and a low flow rate ensures equal temperature in the cells.

4.3. Experiment and data analysis

The generated difference frequency radiation is split into two beams. The first beam passed through the reference cell filled with a calibrated CO_2 gas ($\delta = -7.42$, Cambridge Isotope Laboratories, Inc.) and the second beam passed through the sample cell. The reference and sample signals are measured simultaneously using two MCT detectors and two data acquisition cards. The optical paths of the reference and sample beams must be carefully balanced. However, to minimize the error introduced by the different path lengths, the open-path sections of the sensor (DFG-stage, cell, detectors) are put into a 15 cm × 30 cm × 45 cm box and purged with N_2. This also eliminates the high background caused by atmospheric CO_2. The data channel is also filled sequentially with N_2 to measure the baseline.

Linear regression provides a simple method to evaluate the measured data. The principles of the process can be seen in Fig. 9 (simulated absorption spectra), which shows the corrected absorbance in the reference and sample channels as a function of frequency. The scan windows (both the reference and sample) are divided into two parts so that the lines belonging to the different isotopes can be separated. The absorbance in the reference channel ($^{12}A_r(k)$ and $^{13}A_r(k)$) can be graphed as a function of absorbance in the sample channel ($^{12}A_s(k)$ and $^{13}A_s(k)$). The slope of the fitted linear curve gives the concentration ratios for both isotopes ($^{12}C_{sample}/^{12}C_{re-}$

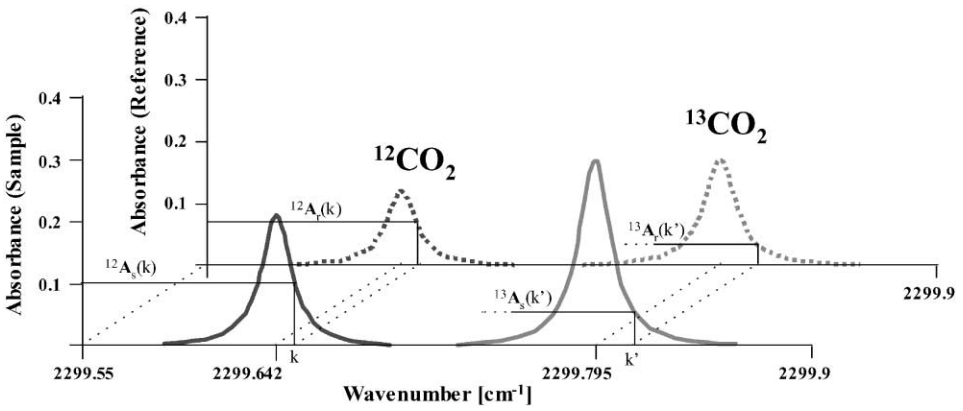

Fig. 9. $^{12,13}CO_2$ absorption spectra for sample and reference gas (see text for details).

ference and $^{13}C_{sample}/^{13}C_{reference}$). Since the isotopic ratio in the reference channel is known ($C \equiv {}^{13}C_{reference}/{}^{12}C_{reference}$), the isotopic ratio in the sample channel can be calculated as

$$\frac{^{13}C_{sample}}{^{12}C_{sample}} = C\,\frac{^{13}Slope}{^{12}Slope}.$$

5. Summary

In summary, five gas species including CO_2, SO_2, HCl, H_2O, and CH_4 were detected using a DFG-based gas sensor and compared with open-path FTIR gas measurements. The DFG-based gas sensor operated with a high resolution and good sensitivity using extractive gas sampling. The sensitivities achieved with both DFG and FTIR instruments are comparable. The continuing development of robust telecom diode laser sources and fiber optic amplifiers will benefit and enable significant improvements of DFG-based gas sensor performance towards smaller physical size, narrower-linewidth and higher DFG power and wavelength coverage. Based on the results obtained in this campaign, future volcanic gas measurements using open-path and isotopic-ratio specific DFG-based gas sensors could offer an attractive means to obtain real-time molar ratios of volcanic gas species, and provide a valuable component of volcano surveillance strategies.

Acknowledgements

This work was partially supported by the UK Natural Environment Research Council (grant number GR9/04655), the Guppo Nazionale per la Vulcanologia (GNV) Framework Program 1999–2001 Coordinated Project (Scientific Coordi-

nator, Dr. P. De Natale), The Robert Welch Foundation and the National Space and Aeronautics Administration (NASA). The authors thank Dr. Rod Jones, University of Cambridge, for discussion, and acknowledge the generous local assistance provided by the Instituto Nicaragüense de Estudios Territoriales (INETER), the Volcán Masaya National Park, and the British embassy, Managua.

References

[1] Tilling RI. Volcanoes. Online edition, URL: http://pubs.usgs.gov/gip/volc/
[2] US Geological Survey Volcano Hazards Program (USGS). URL: http://vulcan.wr.usgs.gov/Volcanoes/Philippines/Pinatubo/images.html
[3] Oppenheimer C, Francis P, Burton M, Maciejewski AJH, Boardman L. Remote measurements of volcanic gases by Fourier transform infrared spectroscopy. Appl Phys B 1998;67(4):505–15.
[4] Francis P, Burton MR, Oppenheimer C. Remote measurements of volcanic gas compositions by solar occultation spectroscopy. Nature 1998;396:567–70.
[5] Richter D, Lancaster DG, Tittel FK. Development of an automated diode laser based multicomponent gas sensor. Appl Opt 2000;39(24):4444–50.
[6] Burton MR, Oppenheimer C, Horrocks LA, Francis PW. Remote sensing of CO_2 and H_2O emission rates from Masaya volcano, Nicaragua. Geology 2000;28:915–8.
[7] United Kingdom Office of National Statistics. URL: http://www.statistics.gov.uk/nsbase/ukin_figs/Data_environment.asp, 2000.
[8] Noguchi, Kimio, Kamiya. Prediction of volcanic eruption by measuring the chemical composition and amounts of gases. Bull Volcanolog 1963;37:367–78.
[9] Flanagan LB, Ehleringer JR. Ecosystem-atmosphere CO_2 exchange: interpreting signals of change using stable isotope ratios. TREE 1998;13(1):10–4.
[10] Craig H. Geochimica et Cosmochimica Acta 1957;12:133–49.
[11] Parello F, Allard P, D'Alessandro W, Federico C, Jean-Baptiste P, Catani O. Isotope geochemistry of Pantelleria volcanic fluids, Sicily Channel rift: a mantle volatile end-member for volcanism in southern Europe. Earth Planet Sci Lett 2000;180:325–39.
[12] Cooper DE, Martinelli RU, Carlisle CB, Risis H, Bour DB, Mena RJ. Measurement of $^{12}CO_2$: $^{13}CO_2$ ratios for medical diagnostics with 1.6-μm distributed-feedback semiconductor diode lasers. Appl Opt 1993;32:6727–31.
[13] Chaux R, Lavorel B. Relative line intensity measurement in absorption spectra using a tunable diode laser at 1.6 μm: application to the determination of $^{13}CO_2/^{12}CO_2$ isotope ratio. Appl Phys B 2001;72:237–40.
[14] Stepanov EV, Zyrianov PV, Miliaev VA. $^{13}CO_2/^{12}CO_2$ ratio analysis in exhaled air by lead-salt tunable diode lasers for noninvasive diagnostics in gastroenterology. SPIE Proc 1999;3829:68–76.
[15] Sauke TB, Becker JF. Stable isotope laser spectrometer for exploration of Mars. Planet Space Sci 1998;46:805–12.
[16] Koplow JP, Goldberg L, Kliner DAV. Compact 1-W Yb-doped double-cladding fiber amplifier using V-groove side pumping. IEEE Photon Technol Lett 1998;10:793–5.
[17] URL: http://www.atm.ox.ac.uk/RFM/
[18] Rodgers CD. Retrieval of atmospheric temperature and composition from remote measurements of thermal radiation. Rev Geophys Space Phys 1976;14:609–24.
[19] McManus JB, Kebabian PL, Zahniser MS. Astigmatic mirror multipass absorption cells for long-path-length spectroscopy. Appl Opt 1995;34:3336–48.
[20] Lancaster DG, Richter D, Tittel FK. Portable fiber-coupled diode-laser-based sensor for multiple trace gas detection. Appl Phys B 1999;69:459–65.